SUPPLEMENTARY INFORMATION

for

Intraplate depth-dependent lithospheric stretching imaged by seismic reflection data

Shuwen Dong[1,2,*], Jianhua Li[3*], Rui Gao[4], Peter A. Cawood[5], Hans Thybo[6],

Yueqiao Zhang[1], Stephen T. Johnston[7], Jinming Wang[3]

[1] *State Key Laboratory for Mineral Deposits Research, Nanjing University, Nanjing 210023, China*
[2] *SinoProbe Center, Chinese Academy of Geological Sciences, Beijing 100037, China*
[3] *Key Laboratory of Paleomagnetism and Tectonic Reconstruction, Ministry of Natural Resources, Institute of Geomechanics, Chinese Academy of Geological Sciences, Beijing 100081, China*
[4] *School of Earth Science and Geological Engineering, Sun Yat-sen University, Guangzhou, 510275, China*
[5] *School of Earth, Atmosphere & Environment, Monash University, Melbourne, VIC 3800, Australia*
[6] *Eurasia Institute of Earth Sciences, Istanbul Technical University, Istanbul, Turkey*
[7] *Earth and Atmospheric Sciences, University of Alberta, Edmonton, Alberta, Canada*

*Correspondence to: swdong8888@126.com; lijianhua0301@126.com

Contents of this file

A. Appendix 1 Detailed descriptions on seismic observations

Northwestern segment. Between CDPs (Common Depth Points) 23000 and 24500, the upper crust shows broadly arcuate packages of finely laminated reflections (A and B, **Fig. 2a**) truncated by NW-dipping sets of high reflections (F_1, F_2 and F_3, **Fig. 2a**), which correlate at surface with folded Ordovician to Triassic strata truncated by NW-dipping thrusts (**Fig. 3a**). F_2 and F_3 flatten with depth, and they merge into a 0.5s-thick, subhorizontal, high-reflective zone interpreted as a decollement (D_1), due to sudden changes in the reflection dip across it (**Fig. 2a**). This decollement and overlying thrusts and folds form a structural pattern indicating southeastward thrust imbrication (**Fig. 3a**).

Beneath CDPs 23000-24000, the middle crust at ~5-9s displays a subhorizontal package of laminar reflections (C) truncated by seismically transparent regions with irregular shapes (**Fig. 2a**), corresponding to Proterozoic layered gneisses truncated by Mesozoic granitoids (Mz_{gr}) (**Fig. 3a**). This reflective package is separated from lower-crustal reflections by a gentle-dipping reflector interpreted as a decollement (D_6, **Fig. 3a**). To the southeast, a set of gently, SE-dipping reflections (D_2) extends from CDP 27000 at ~7s to CDP 24000 at ~4s (**Fig. 2a**). This reflective set progressively steepens upward by truncating underlying subhorizontal reflections to the northwest, and it finally approaches D_1 (**Fig. 2a**), forming critical-taper wedges capable of accommodating contractional strain transfer between the upper and middle crust (**Fig. 3a**).

Central Segment. Between CDPs 24500 and 25000, fine-laminated reflections at 0-1.5s, bounded by the Qiyang fault (F_{11}), dip increasingly southeastward and form a

wedge-shaped geometry (**Fig. 2a**); they correspond to the Cretaceous growth strata onlapping the folded Paleozoic strata within the half-graben. Along-strike variations of strata across the Qinyang fault (**Fig. 3a**) suggest that the normal faulting may have exploited an older thrust due to pre-existing rheological weakness.

To the southeast (CDPs 26000-29500), the upper crust contains finely-laminated, gentle-dipping reflections underlain by whitish, less-reflective domains (**Fig. 2b**). The laminar reflections correspond to the Cretaceous strata within the Hengyang basin (**Fig. 2a**). They are discontinuous due to truncations by a series of NW- and SE-dipping normal faults. Normal faulting resulted in an interior-facture structural pattern of the basin (**Fig. 2b**). Beneath the whitish appearance (CDPs 28500-29500), a gentle-dipping, high-reflective set is underlain by another set of SE-dipping reflections (**Fig. 2a**); their contact (U) corresponds to the angular unconformity at the base of the Devonian strata based on surface geology (**Fig. 3a**).

Southeastern Segment. Between CDPs 29500 and 31500, several NW- and SE-dipping thrusts (F_6-F_9, Fig. 2a) could be traced via their seismic manifestations of transparent or diffractive zones that (1) disrupt laterally coherent reflections, or (2) separate regions of contrasting reflection dips.

Further to the southeast (CDPs 31500-33000), three mid-crustal reflections (D_3, D_4 and D_5) exhibit flat-ramp-flat trajectories resembling decollements (**Fig. 2a**). Sudden changes in reflection dip occur across their ramps, where underlying subhorizontal reflections are truncated by the ramps, whereas overlying reflections are parallel to the ramps (**Fig. 2a**). Folding of hanging-wall reflections forms thrust-

ramp folds. Such structural relationships suggest a thin-skinned thrust-and-fold system with multiple decollements (**Fig. 2a**). Around CDP31000, a set of high-amplitude reflections is cut by the Yongxing fault (F_{10}), forming a ~1.5s normal-sense offset (**Fig. 2a**); normal faulting generated the Yongxing basin (**Fig. 3a**), documenting extensional overprinting of the thrust system.

B. Supplementary figures S1-S6

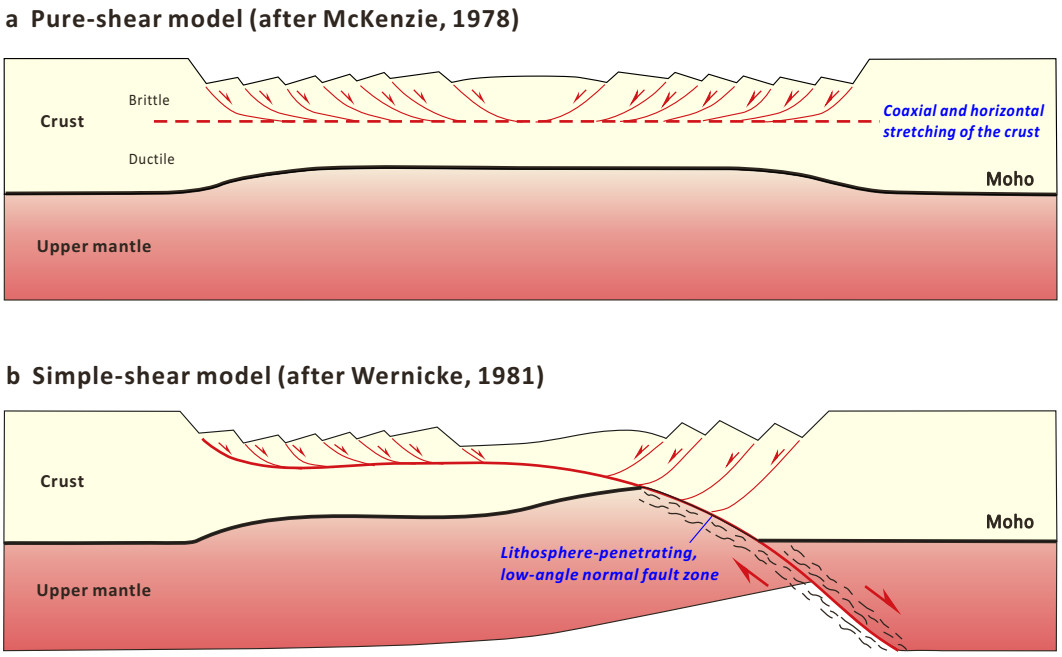

Fig. S1 Two mechanisms for extension of the continental lithosphere. a, the pure-shear mechanism highlights in site, coaxial, and horizontal stretching, accompanied by vertical thinning during lithospheric extension[11]. **b,** the simple-shear mechanism assumes the extension to be mostly accommodated by non-coaxial faulting along a low-angle, lithosphere-penetrating fault zone, which links crustal displacements over large-scale discrete areas[1].

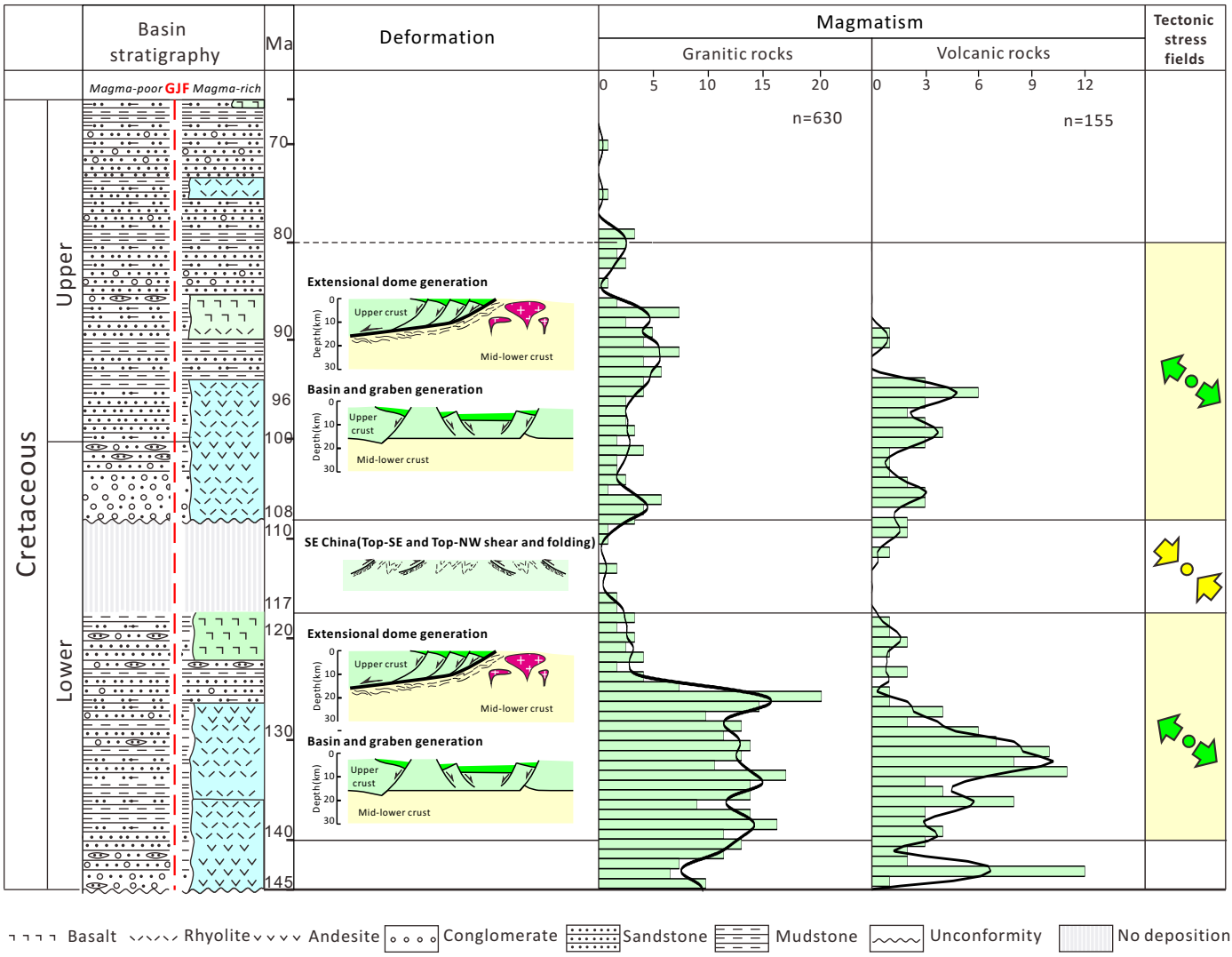

Fig. S2 Reconstruction of Cretaceous evolution of South China. This reconstruction is based on a compilation of sedimentary archives, analyses of structural data sets and tectonic stress fields, and magmatic activities.

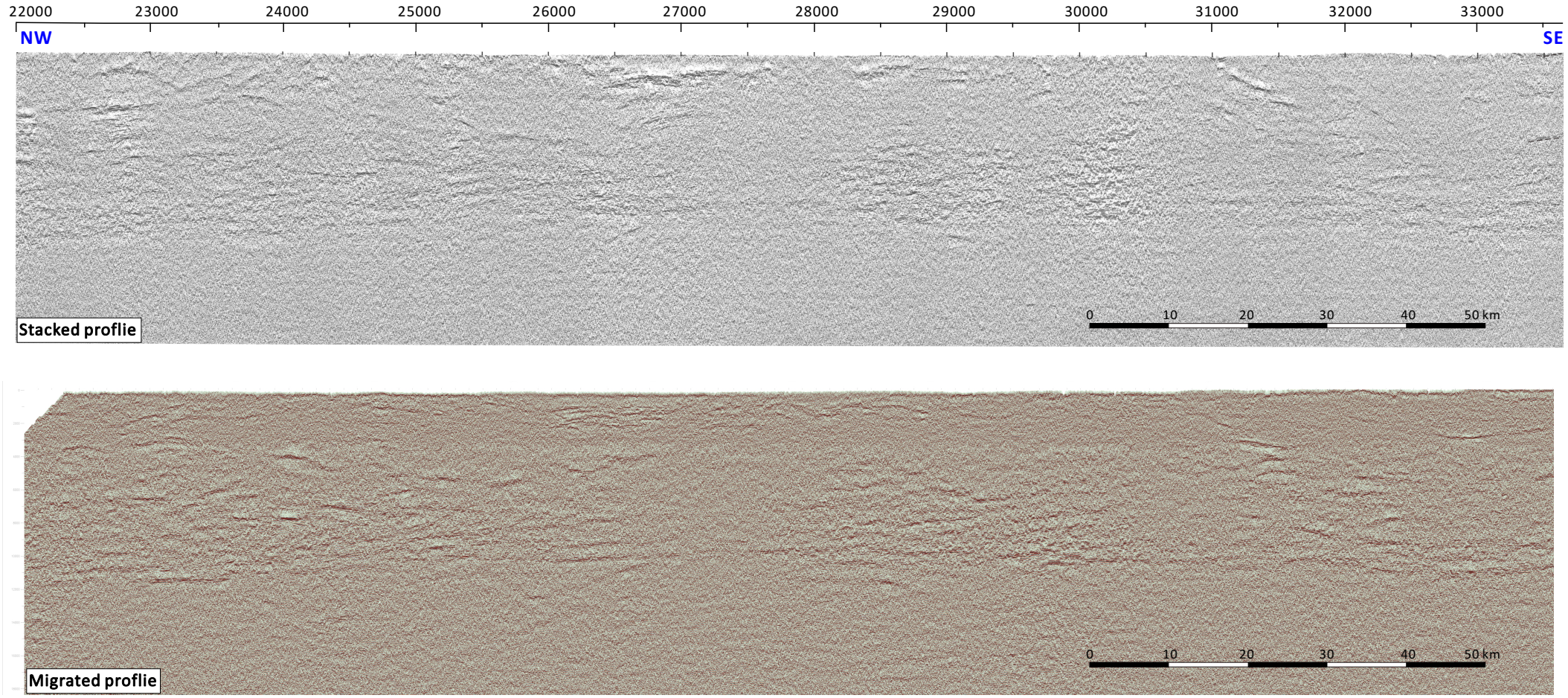

Fig. S3 Migrated and stacked seismic profiles without line drawing.

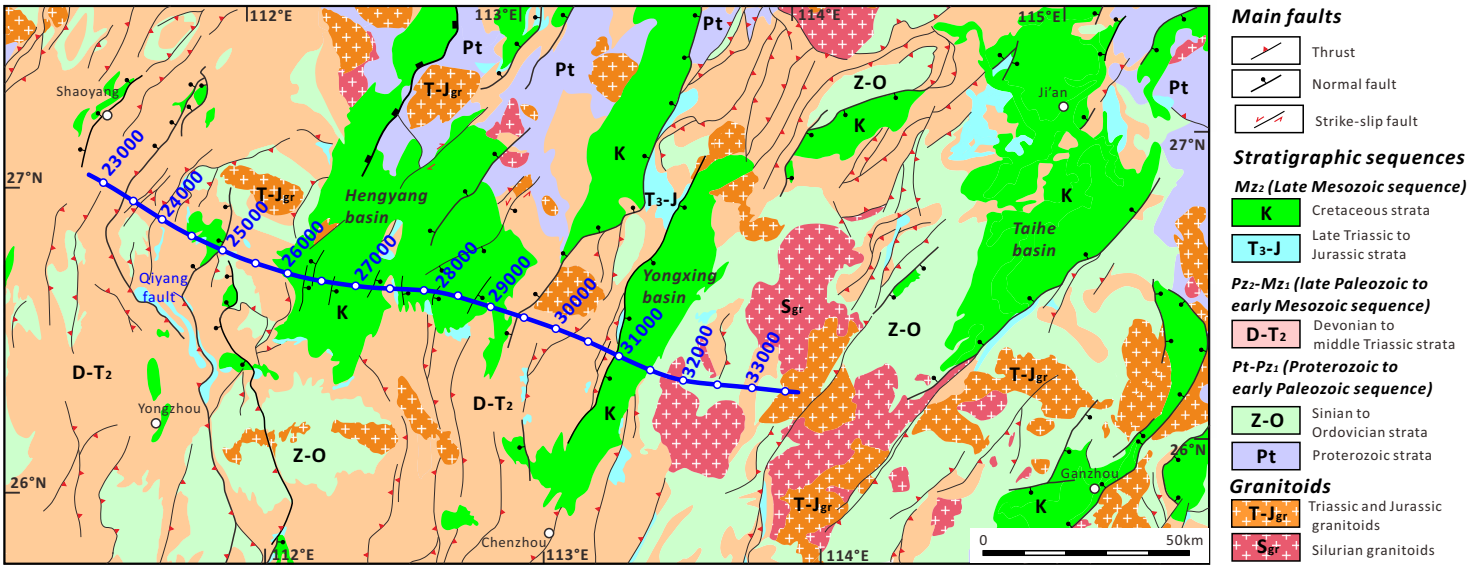

Fig. S4 Simplified geological map showing surface structures and magmatic rocks along the seismic profile.

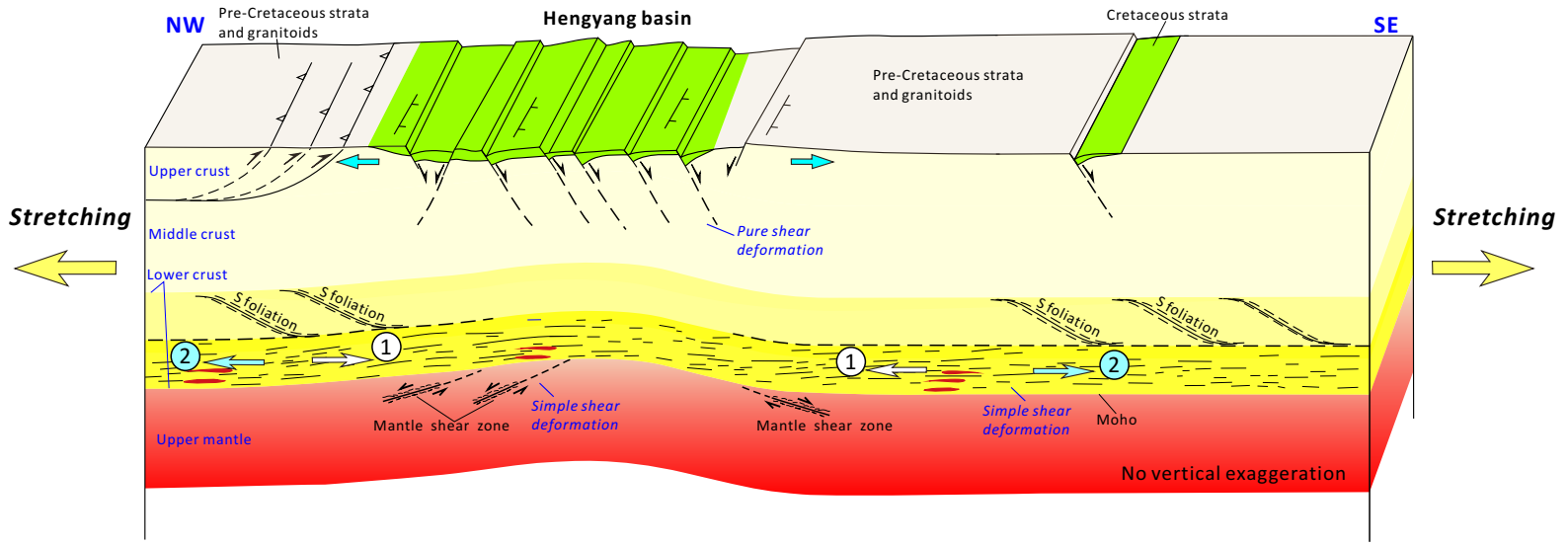

Fig. S5 A cartoon showing main extensional features of upper lithosphere of central South China.

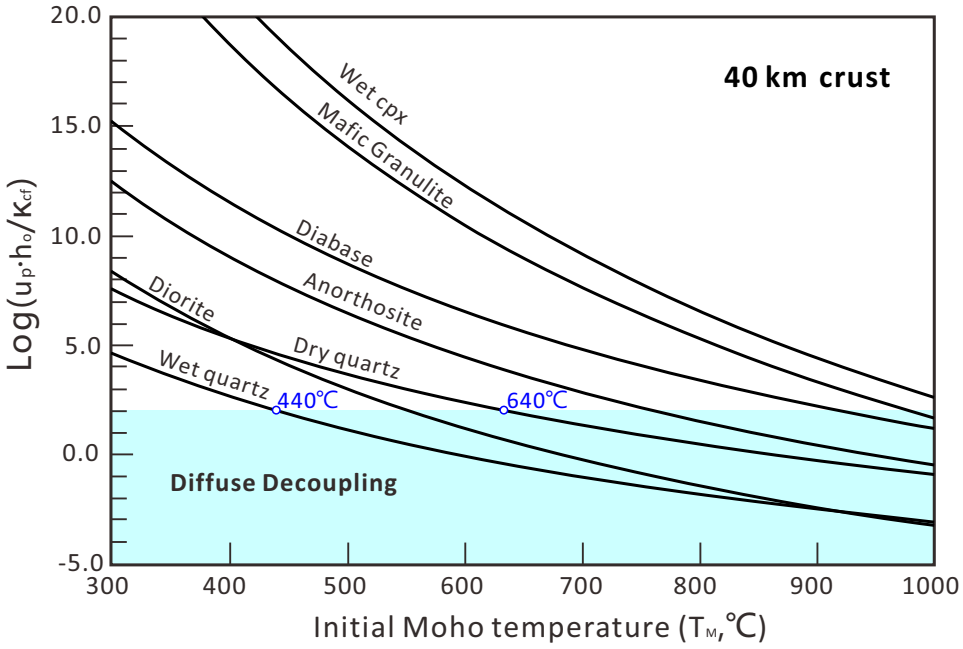

Fig. S6 Plots of $u_p \cdot h_0/k_{cf}$ vs the initial Moho temperature (T_M) for an average ~40-km-thick crust. k_{cf}, the diffusion constant; u_p, the plate spreading velocity; h_0, the crustal thickness. The diffuse decoupling occurs when the ratio of $u_p \cdot h_0/k_{cf} < 100$[30], as indicated by the shaded region. See refs. 30 and 31 for details of governing equations.

C. Supplementary table S1

Governing equations and parameters for calculating the T_M for the ~40-km-thick crust

Studies on governing equations demonstrate that the diffuse decoupling occurs when the ratio of $u_p \cdot h_0/\kappa_{cf} < 100$, where κ_{cf} is the diffusion constant, u_p is the plate spreading velocity, h_0 is the crustal thickness[30]. We calculate the initial Moho temperature (T_M) by plotting $log(u_p \cdot h_0/\kappa_{cf})$ vs T_M using the following equations from refs. 30, 31: $\kappa_{cf} = \frac{g\Delta\rho^* y_0^3}{\eta_0}$, where κ_{cf} is the effective diffusivity for crustal flow, g is the acceleration of gravity, $\Delta\rho^*$ is the density contrast, equal to $\rho_c(\rho_m-\rho_c)/\rho_m$, ρ_c is the crustal density, ρ_m is the mantle density, y_0 is the length scale for e-folding of crustal viscosity, η_0 is effective crustal viscosity at Moho. Among them, $y_0 = \frac{RT_M^2}{E(\partial T/\partial z)}$, where T_M is the temperature at Moho, R is the universal gas constant, E is activation energy, $\partial T/\partial z$ is the thermal gradient; $\eta_0 = C\exp\left(\frac{E}{RT_M}\right)$, where C is the activation volume.

Material	Rheological parameters					Ref.
	Flow law / reference	$A(Pa^{-n}\cdot s^{-1})$	n	$E(KJ\cdot mol^{-1})$	$C(Pa\cdot s)$	
Upper crust	wet quartzite	1.30×10^{-20}	2.4	134	3.1×10^{11}	51
	dry quartzite	5.00×10^{-25}	2.9	149	8×10^{12}	52
	diabase	7.96214×10^{-25}	3.4	260	5×10^{9}	53
Lower crust	anorthosite	5.60×10^{-23}	3.2	238	1.1×10^{9}	54
	wet cpx	2.34423×10^{-15}	3.3	490	6.760829754	55
	wet diorite	1.27394×10^{-16}	2.4	212	3.125×10^{7}	56

	dry mafic granulite	8.8334×10^{-22}	4.2	445	71.42857143	57

Here *A* is the material constant of power flow law, *n* is the power law stress exponent, *E* is activation energy, *C* is the activation volume.

Our results (**Fig. S6**) demonstrate that, for both wet and dry ~40 km thick quartz crust, the diffuse decoupling herein occurred at T_M ~440-640 ℃, comparable to that of non-volcanic passive margins[32].

References

51. Kronenberg, A. K. & Tullis, J. Flow strengths of quartz aggregates: grain size and pressure effects due to hydrolytic weakening. *Journal of Geophysical Research Solid Earth* **89,** 4281- 4297 (1984).
52. Koch, P. S. Rheology and microstructures of experimental deformed quartz aggregates (flow laws, piezometry, rock mechanics). *University of California, Los Angeles* (1983).
53. Kirby, S.H. Rheology of the lithosphere. *Reviews of Geophysics* **21,** 1458-1487 (1983).
54. Shelton, G. & Tullis, J. Experimental flow laws for crustal rocks. *European Seismological Commission Meeting* **62,** 396 (1981).
55. Boland, J.N. & Tullis, T.E. Deformation behavior of wet and dry clinopyroxenite in the brittle to ductile transition region. *American Geophysical Union (AGU)* (1986).
56. Ranalli, G. Rheology of the Earth: London. *Chapman and Hall* **413 p** (1995).
57. Wilks, K. R. & Carter, N. L. Rheology of some continental lower crustal rocks. *Tectonophysics* **182,** 57-77 (1990).